Kinetically controlled, adhesiveless transfer printing using microstructured stamps

Tae-Ho Kim,[1] Andrew Carlson,[1] Jong-Hyun Ahn,[2] Sang Min Won,[3] Shuodao Wang,[4] Yonggang Huang,[4,5] and John A. Rogers[1,3,6,a)]

[1]*Department of Materials Science and Engineering, Beckman Institute, and Frederick Seitz Materials Research Laboratory, University of Illinois at Urbana-Champaign, Illinois 61801, USA*
[2]*School of Advanced Materials Science and Engineering, SKKU Advanced Institute of Nanotechnology, Sungkyunkwan University, Suwon 440-746, Republic of Korea*
[3]*Department of Electrical and Computer Engineering, University of Illinois at Urbana-Champaign, Illinois 61801, USA*
[4]*Department of Mechanical Engineering, Northwestern University, Evanston, Illinois 60208, USA*
[5]*Department of Civil and Environmental Engineering, Northwestern University, Evanston, Illinois 60208, USA*
[6]*Department of Chemistry, University of Illinois at Urbana-Champaign, Illinois 61801, USA*

(Received 17 December 2008; accepted 24 February 2009; published online 16 March 2009)

This letter describes the physics and application of an approach to transfer printing that uses stamps with microstructures of relief embossed into their surfaces. Experimental measurement of velocity-dependent adhesive strength as a function of relief geometry reveals key scaling properties and provides a means for comparison to theoretical expectation. Formation of transistor devices that use nanoribbons of silicon transfer printed directly onto glass substrates without adhesive layers demonstrates the use of this type of approach for a high-performance (mobilities >325 $cm^2/V\ s$ and on/off ratios $>10^5$) single crystal silicon on glass technology. © *2009 American Institute of Physics*. [DOI: 10.1063/1.3099052]

Elastomeric materials such as polydimethylsiloxane (PDMS) have been widely used as stamps for transfer printing solid objects (e.g., semiconducting nanomaterials, single-walled carbon nanotubes, microdevices, and others) from surfaces on which they are fabricated to foreign substrates such as semiconductor wafers, glass plates, plastic sheets, and rubber slabs.[1–4] In the most robust version of this process, adhesion to the stamp arises from nonspecific, van der Waals interactions, while that to the target substrate is mediated by an adhesive, such as a photocurable polymer.[5,6] A more interesting and valuable process exploits the viscoelastic nature of the stamps to control adhesion through peeling rate, whereby inking and printing can be accomplished at high and low peel rates, respectively, without any adhesives.[3] This operation requires that the strength of ink adhesion to the target substrate is sufficiently large to overcome the van der Waals adhesion to the stamp, even in the limit of slow peeling. Such printing sometimes presents a practical challenge due to the reduced contact areas between many "inks" and target substrates compared to contact between inks and soft, conformable stamps. This paper demonstrates the use of microscale surface relief on stamps as a means to reduce contact area with a nanoribbon ink, in a manner that can reduce the adhesion and facilitate printing. High yield printing of single crystal silicon nanoribbons onto glass substrates for high performance transistors provides an example application in silicon on glass (SOG) electronics.[7,8]

Figure 1(a) presents a schematic illustration of adhesiveless transfer printing with a stamp containing a line and space surface relief geometry. Here, the ink consists of thin ribbons of silicon with lengths much larger than the width of the stamp relief structures. After contacting the stamp against the ink, the nanoribbons are separated from the donor substrate by removing the stamp with a high peeling rate.[3] Placing the inked stamp in contact with a flat target substrate, and then removing at low peeling rate affects transfer and completes the process. The reduced contact area associated with the relief structure facilitates release to achieve overall yields that are greater than possible with flat stamps. The fabrication process for such structured stamps exploits the well developed casting and curing techniques of soft lithography, using layers of photoresist (SU8–2, MicroChem Corp.) on silicon wafers as templates for PDMS stamps. Surface and cross-sectional scanning electron microscope (SEM) images of a representative structured stamp made by this procedure appear in Figs. 1(b) and 1(c), respectively. By varying the

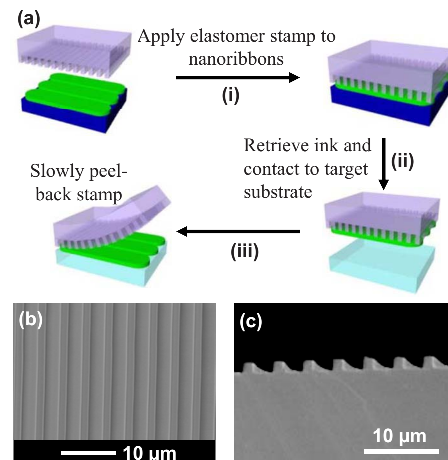

FIG. 1. (Color online) (a) Schematic illustration of the transfer printing process using a structured stamp. (b) Top view SEM image of a representative stamp of this type. (c) Cross-sectional SEM image of the stamp.

a)Electronic mail: jrogers@uiuc.edu.

 © 2009 American Institute of Physics

Downloaded 18 Mar 2009 to 202.20.192.250. Redistribution subject to AIP license or copyright; see http://apl.aip.org/apl/copyright.jsp

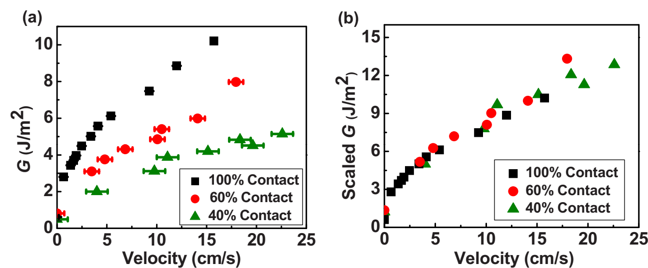

FIG. 2. (Color online) Velocity-dependent adhesive strength of structured PDMS stamps with different contact areas. (a) Three curves representing the cases of 100% (squares; flat stamp), 60% (circles; line and space stamp), and 40% (triangles; line and space stamp) contact areas. The peel direction in all cases was perpendicular to the surface relief structures. Error bars represent the standard deviation in delamination velocity for each applied load. (b) Common adhesion curve for all stamps measured.

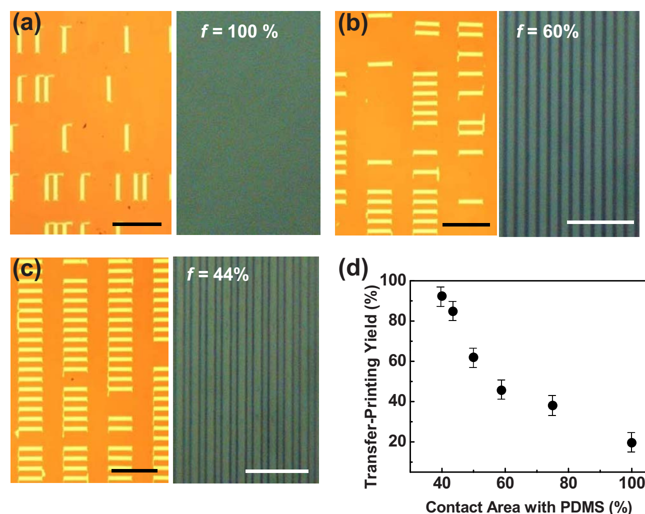

FIG. 3. (Color online) [(a)–(c)] Left panel: top view optical images of arrays of 300 nm thick Si ribbons transfer printed onto a glass substrate by the PDMS stamps shown in the right panels. Contact areas f for the stamps are: (a) 100% (flat surface), (b) 60% (line/space relief), and (c) 44% (line/space relief). Scale bars for all ribbon array images is 200 μm and for stamp images is 10 μm. (d) Printing yield as a function of the contact area between structured PDMS stamps and Si ribbons.

geometry of the photoresist patterns, stamps with nearly any ratio of raised to recessed regions can be produced. In well designed systems only the raised regions make contact with the ink and this contact area, as defined by the coverage of raised regions, is a critical parameter that controls the strength of adhesion between the stamp and the ink.

For high yield printing of nanoribbons, the relative adhesive strength of the ink to the stamp must be less than that to the substrate layer.[9] The former quantity can be evaluated explicitly by determining the energy released during separation of the ribbons from the stamp at a steady-state velocity.[3,9–12] In a simple tape peel test, this energy release rate G is related to the stamp width w, and the applied force F by $G=F/w$. Due to stamp viscoelasticity, the energy release rate at the ink/stamp interface is strongly velocity-dependent, i.e., $G^{\text{ink/stamp}}(v)$.[9,13–15] Thus, to print, this energy release rate must be less than the corresponding G-value between the nanoribbons and the target substrate $G^{\text{ink/stamp}}(v) < G^{\text{ink/target}}$. For most cases where the ink and target are nonviscoelastic, $G^{\text{ink/target}}$ is constant.[3,9] In a similar analysis to Feng *et al.*,[9] who studied noncontinuous contacting ink/stamp layers (i.e., segmented inks or patterned stamps), the average energy release rate, in the absence of contact between substrate and stamp, will be related to the contact area f at the stamp/ink interface, $G_{\text{print}}=fG^{\text{ink/stamp}}(v)$. This suggests that the adhesive strength for the stamp/nanoribbon/substrate system should scale proportionally with the contact area.

90° peel tests[9,11,13] were conducted to determine quantitatively the stamp adhesive strength as a function of contact area with a continuous ink layer. Patterned PDMS stamps 1 mm thick were cleaned with ethanol, dried under nitrogen, and laminated against a 1 mm thick glass slide (Fisher Scientific) coated with gold (100 nm). Applying constant loads to one end of the stamp initiated delamination from the gold film. The distance traveled by the delamination front, the point of separation between the stamp and ink layer, and time were obtained by video recordings of each peeling event. From the resulting displacement-time profiles, steady-state separation velocities were determined for each applied load with the corresponding energy release rates calculated from the load and stamp width. Figure 2(a) illustrates the velocity-dependent energy release rate for a flat stamp (100% contact) and for structured stamps having 60% contact area (lines, 30 μm widths, 20 μm spaces, 15 μm depth) and 40% contact area (lines, 20 μm widths, 30 μm spaces, 15 μm depth). Qualitatively, decreasing the contact area leads to a corresponding decrease in the adhesive strength. Removing contact area effects by dividing the velocity-dependent energy release rates by f reveals a common master adhesion curve, as shown in Fig. 2(b). The results, while validating a basic prediction of the theory, may not exhibit the same level of quantitative agreement for all relief geometries and peel directions. However, the general trend toward lower adhesion for lower contact area should remain valid for relief features of a given type.

Adhesion reduction through contact area can be used to advantage for printing, as demonstrated in Fig. 3 with stamps having different relief patterns. The left panels of Figs. 3(a)–3(c) show optical micrographs of arrays of 300 nm thick single crystal Si nanoribbons (20 μm width and 100 μm length) printed onto glass substrates by the stamps imaged in the corresponding right panels. For the flat stamp of Fig. 3(a) (100% contact area) the transfer printing yield is 20%. However, for the patterned regions of Fig. 3(b) (lines, 1 μm widths, 0.7 μm spaces, 1.5 μm depth, 60% contact area) and Fig. 3(c) (lines, 1 μm widths, 1.3 μm spaces, 1.5 μm depth, 44% contact area) the printing yield is 46% and 85%, respectively. In all cases, peeling was perpendicular to the relief features on the stamp and yields were limited by printing rather than the inking part of the process. Additional measurements of this type, shown in Fig. 3(d), provide a more complete relationship between the yield (percent) and contact area (percent).

Interfacial contact area also influences the efficacy of both the inking and printing steps in the total transfer printing process. For efficient inking, f must be greater than $f_{\min}=G^{\text{ink/donor}}/G(v_{\max})$, a system-dependent minimum contact area necessary for ink retrieval. $G^{\text{ink/donor}}$ and $G(v_{\max})$ are the energy release rates at the ink/donor interface and at maximum peeling velocity $\nu_{\max}$, respectively. For the grating structures examined here, complete retrieval of ribbons (i.e., inking) occurred with stamps having at least 40% contact area; below this threshold, adhesion to the stamp was not

Downloaded 18 Mar 2009 to 202.20.192.250. Redistribution subject to AIP license or copyright; see http://apl.aip.org/apl/copyright.jsp

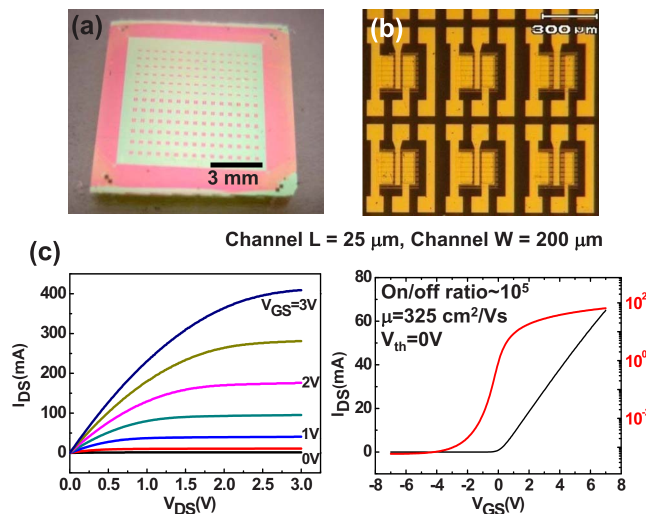

FIG. 4. (Color online) (a) Photograph of a 300 nm thick phosphorus-doped silicon membrane printed onto a glass substrate without an adhesion layer. (b) Optical images of an array of single-crystal silicon TFTs fabricated on this membrane with a SiO_2 gate dielectric layer (100 nm thick) and source, drain and gate electrodes of Cr/Au (3/100 nm). (c) Full current-voltage and transfer (source/drain bias=0.1 V) characteristics of devices with channel lengths and widths of 25 and 200 μm, respectively.

sufficiently strong. In a similar manner, the contact area for printing structures must be smaller than $f_{max}=G^{ink/target}/G_0$, where G_0 is an empirical zero-velocity critical energy release rate;[9,13,14] values of f greater than this maximum result in incomplete release from the stamp. In the case of the 1 μm line width/1.5 μm space stamp (40% contact area), the yield for the full process (i.e., inking and printing) was maximized at 92.4%. This value does not represent an upper limit, but rather an optimal case for the particular stamp and nanoribbon geometry examined here. For example, larger or interconnected ribbons can have process yields which are much higher [>99%, as shown in Fig. 4(a)].

To demonstrate the practical value of this approach, we fabricated transistors using single crystal Si printed onto glass via an optimized structured stamp. Figure 4(a) shows an example of a printed *n*-doped Si nanomembrane, in which the regular array of shaded patterns corresponds to the phosphorus-doped regions. Figure 4(b) shows devices formed with a gate dielectric of SiO_2 (100 nm thickness; deposited by plasma enhanced chemical vapor deposition (PECVD) with SiH_4 and N_2O at 250 °C) and source, drain, and gate electrodes of Cr/Au deposited by electron beam evaporation (Temescal BJD1800). The resulting thin film transistors (TFTs) show accumulation mode *n*-channel transistor behavior, as indicated by the current-voltage characteristics in Fig. 4(c). The channel length of this device is 25 μm with a corresponding width of 200 μm. The transfer characteristics presented in Fig. 4(c) indicate a threshold voltage of ~0 V, an effective mobility of 325 cm²/V s, and device on/off ratios typically $>10^5$. These results could be relevant to the development of an unusual type of SOG technology. The same approaches can also be valuable for printing other classes of materials (e.g., GaAs, GaN, etc.) onto other classes of substrates (e.g., semiconductor wafers, plastic sheets, etc), a process of particular utility for systems that demand intimate contact between the printed materials and the underlying substrate without intervening adhesive layers.

We thank T. Banks for helping with e-beam lithography and processing using facilities at the Frederick Seitz Materials Research Laboratory (MRL). This work was supported in part by MURI Grant No. FA9550–08–1-0337. The general characterization facilities were provided through MRL with support from the University of Illinois and from DOE Grant Nos DE-FG02–07ER46453 and DE-FG02–07ER46471. T.-H.K. acknowledges the Korea Research Foundation Grant No. KRF-2006–214-D00044, funded by the Korean Government (MOEHRD). A.C. acknowledges support from the Department of Defense (DOD) through the National Defense Science and Engineering Graduate (NDSEG) Fellowship program. T.-H.K. and A.C. contributed equally to this work.

[1]J.-H. Ahn, H.-S. Kim, K. J. Lee, S. Jeon, S. J. Kang, Y. Sun, R. G. Nuzzo, and J. A. Rogers, Science **314**, 1754 (2006).
[2]S.-H. Hur, D.-Y. Khang, C. Kocabas, and J. A. Rogers, Appl. Phys. Lett. **85**, 5730 (2004).
[3]M. A. Meitl, Z.-T. Zhu, V. Kumar, K. J. Lee, X. Feng, Y. Y. Huang, I. Adesida, R. G. Nuzzo, and J. A. Rogers, Nature Mater. **5**, 33 (2006).
[4]T.-H. Kim, W. M. Choi, D.-H. Kim, M. A. Meitl, E. Menard, H. Jiang, J. A. Carlisle, and J. A. Rogers, Adv. Mater. (Weinheim, Ger.) **20**, 2171 (2008).
[5]E. Menard, R. G. Nuzzo, and J. A. Rogers, Appl. Phys. Lett. **86**, 093507 (2005).
[6]J. Yoon, A. J. Baca, S.-I. Park, P. Elvikis, J. B. Geddes, L. Li, R. H. Kim, J. Xiao, S. Wang, T. H. Kim, M. J. Motala, B. Y. Ahn, E. B. Duoss, J. A. Lewis, R. G. Nuzzo, P. M. Ferreira, Y. Huang, A. Rockett, and J. A. Rogers, Nature Mater. **7**, 907 (2008).
[7]K. P. Larsen, J. T. Ravnkilde, and O. Hansen, Proceedings on the 12th International Conference on TRANSDUCERS, Solid-State Sensors, Actuators and Microsystems, 2003 (unpublished), Vol. 2, p. 1655–1658.
[8]J. Chae, H. Kulah, and K. Najafi, J. Micromech. Microeng. **15**, 336 (2005).
[9]X. Feng, M. A. Meitl, A. M. Bowen, Y. Huang, R. G. Nuzzo, and J. A. Rogers, Langmuir **23**, 12555 (2007).
[10]A. Majumder, A. Ghatak, and A. Sharma, Science **318**, 258 (2007).
[11]A. N. Gent and S.-M. Lai, J. Polym. Sci., Part B: Polym. Phys. **32**, 1543 (1994).
[12]T. L. Anderson, *Fracture Mechanics: Fundamentals and Applications*, 2nd ed. (CRC, Boca Raton, 1995).
[13]A. N. Gent, Langmuir **12**, 4492 (1996).
[14]K. Kendall, Science **263**, 1720 (1994).
[15]K. S. Kim and J. Kim, ASME J. Eng. Mater. Technol. **110**, 266 (1988).

Downloaded 18 Mar 2009 to 202.20.192.250. Redistribution subject to AIP license or copyright; see http://apl.aip.org/apl/copyright.jsp